Vol. 22, e220014 (2025)
doi: 10.2142/biophysico.bppb-v22.0014

Biophysics and Physicobiology
https://www.jstage.jst.go.jp/browse/biophysico/

Regular Article

HulaChrimson: A Chrimson-like cation channelrhodopsin discovered using freshwater metatranscriptomics from Lake Hula

Hiroto Takahashi[1], Shunki Takaramoto[1], Takashi Nagata[1], Shai Fainsod[2], Yoshitaka Kato[1], Oded Béjà[2,3], Keiichi Inoue[1]

[1] *The Institute for Solid State Physics, The University of Tokyo, Kashiwa, Chiba 277-8581, Japan*
[2] *Faculty of Biology, Technion — Israel Institute of Technology, Haifa 3200003, Israel*
[3] *The Nancy and Stephen Grand Technion Energy Program (GTEP), Technion—Israel Institute of Technology, Haifa 3200003, Israel*

Received April 14, 2025; Accepted July 3, 2025;
Released online in J-STAGE as advance publication July 5, 2025
Edited by Hironari Kamikubo

Chrimson is cation-conducting channelrhodopsin (CCR) with the most red-shifted absorption spectrum, rendering itself as one of the most promising optogenetic tools. However, the molecular mechanisms underlying its red-shifted absorption have not been completely clarified yet. Here, we found a CCR gene showing high sequence similarity to Chrimson from Lake Hula through freshwater metatranscriptome sampling. Interestingly, despite its high similarity to Chrimson, this CCR—named HulaChrimson—showed significantly blue-shifted action and absorption spectra compared to those of Chrimson. Mutations of amino acid residues, which are prominently different from those in Chrimson, in HulaChrimson did not reproduce the red-shifted absorption of Chrimson, suggesting the color-tuning between these proteins achieved by organizing the entire protein architecture, particularly in the broad hydrogen bonding network around the retinal Schiff base counterion, rather than by the difference in several specific residues. The optical characteristics of HulaChrimson distinct from those of Chrimson provide a basis for understanding the color-tuning mechanisms of channelrhodopsins.

Key words: Channelrhodopsin, retinal, patch clamp, color tuning

Significance

A channelrhodopsin named HulaChrimson, having an amino-acid sequence highly similar to that of Chrimson, was found through a freshwater metatranscriptome sampling. Interestingly, HulaChrimson exhibits action and absorption spectra significantly blue-shifted from those of Chrimson. The large difference in the absorption spectra between HulaChrimson and Chrimson along with their similar amino acid sequences provide us a basis for understanding the mechanisms underlying the color-tuning among channelrhodopsins.

Introduction

Microbial rhodopsins are photoreceptive membrane proteins using an all-*trans*-retinal (ATR) chromophore incorporated in a seven or eight-transmembrane helical architecture [1-3]. While microbial rhodopsins elicit a variety of biological functions in a light-dependent manner, channelrhodopsins (ChRs) function as light-gated ion channels [4,5]. These proteins are classified into four distinct groups: (1) cation-conducting ChRs from chlorophytes (chlorophyte CCR) and (2) cryptophytes (cryptophyte CCR), (3) microbial rhodopsins from giant viruses, including cation-conducting ChRs and

Corresponding author: Keiichi Inoue, The Institute for Solid State Physics, The University of Tokyo, Kashiwa, Chiba 277-8581, Japan. ORCID iD: https://orcid.org/0000-0002-6898-4347, e-mail: inoue@issp.u-tokyo.ac.jp

outward proton pumps (viral rhodopsins), and (4) anion-conducting ChRs (ACRs) from diverse algae, protists, and giant viruses (Figure 1A). Based on their amino acid sequence similarity to proton-pumping rhodopsins, including bacteriorhodopsin from *Halobacterium salinarum* (*Hs*BR), cryptophyte CCRs are also referred to bacteriorhodopsin-like CCRs or pump-like CCRs. These ChRs are used in optogenetics to optically control the activity of excitable cells including neurons or intracellular ion balance in plant cells [6-9]. While channelrhodopsin-2 from *Chlamydomonas reinhardtii* (*Cr*ChR2) is being most widely used, *Cr*ChR2 has several characteristics—short wavelength absorption, low ion conductance, significant desensitization upon prolonged illumination and so on—which are not suitable for its usage as an optogenetic tool. To solve these limitations, ChRs showing better molecular properties have been explored through genome mining and artificial protein engineering [10-21]. Among them, Chrimson from *Chlamydomonas noctigama* has been known for its most red-shifted absorption as CCR, whose action spectrum of photocurrent peaks at 590 nm [22-24]. Since long-wavelength light causes less photo damage and is less scattered by biological tissues, enabling penetration into deeper tissues, the red-shifted absorption of Chrimson is highly useful for optogenetics.

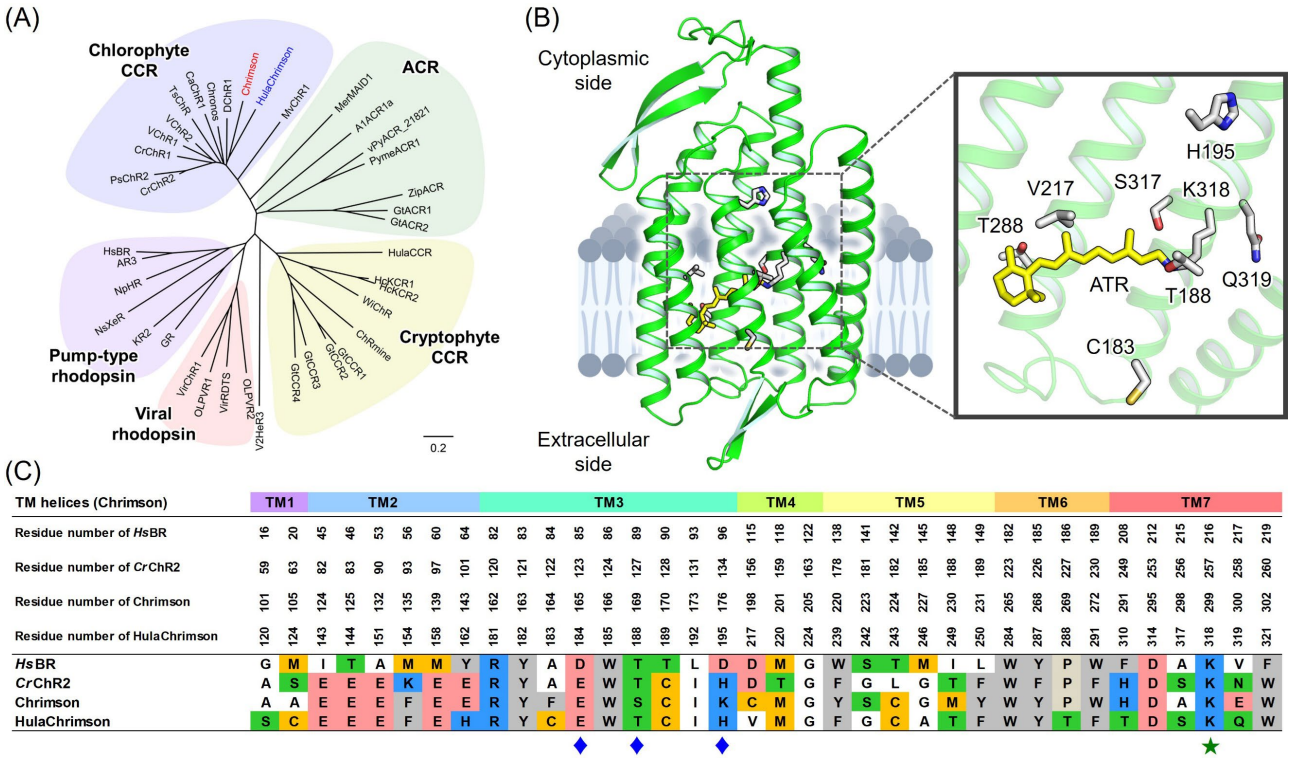

(C)

TM helices (Chrimson)	TM1		TM2							TM3									TM4			TM5										TM6					TM7								
Residue number of *Hs*BR	16	20	45	46	53	56	60	64	82	83	84	85	86	89	90	93	96	115	118	122	138	141	142	145	148	149	182	185	186	189	208	212	215	216	217	219								
Residue number of *Cr*ChR2	59	63	82	83	90	93	97	101	120	121	122	123	124	127	128	131	134	156	159	163	178	181	182	185	188	189	223	226	227	230	249	253	256	257	258	260								
Residue number of Chrimson	101	105	124	125	132	135	139	143	162	163	164	165	166	169	170	173	176	198	201	205	220	223	224	227	230	231	265	268	269	272	291	295	298	299	300	302								
Residue number of HulaChrimson	120	124	143	144	151	154	158	162	181	182	183	184	185	188	189	192	195	217	220	224	239	242	243	246	249	250	284	287	288	291	310	314	317	318	319	321								
*Hs*BR	G	M	I	T	A	M	M	Y	R	Y	A	D	W	T	T	L	D	D	M	G	W	S	T	M	I	L	W	Y	P	W	F	D	A	K	V	F								
*Cr*ChR2	A	S	E	E	E	K	E	E	R	Y	A	E	W	T	C	I	H	D	T	G	F	G	L	G	T	F	W	F	P	F	H	D	S	K	N	W								
Chrimson	A	A	E	E	E	F	E	E	R	Y	F	E	W	S	C	I	K	C	M	G	Y	S	C	G	M	Y	W	Y	P	W	H	D	A	K	E	W								
HulaChrimson	S	C	E	E	E	F	E	H	R	Y	C	E	W	T	C	I	H	V	M	G	F	G	C	A	T	F	W	Y	T	F	T	D	S	K	Q	W								

Figure 1 Phylogenetic analysis and structural features of HulaChrimson.
(A) The phylogenetic tree of representative ion-pumping rhodopsins, channelrhodopsins, viral rhodopsins, heliorhodopsin, and HulaChrimson. The phylogenetic tree was inferred using the neighbor-joining method of MEGA 6 software. The positions of amino acids in TM1 and TM2 were manually corrected based on the X-ray crystallographic structures. (B) Schematic illustration of HulaChrimson structure based on AlphaFold 3 prediction. The position of ATR is shown based on the X-ray crystallographic structure of Chrimson (PDB ID: 5ZIH [24]) (C) Amino acid sequence alignment of HulaChrimson with *Hs*BR, *Cr*ChR2, and Chrimson. The amino acids are colored according to their chemical properties: hydrophobic aliphatic residues and Gly (white); hydroxyl group-bearing aliphatic residues, Asn, and Gln (green); acidic residues (red); basic residues (blue); sulfur-containing residues (orange); proline (light gray); aromatic residues (gray). The positions of TMs were indicated by colored rectangles, based on the X-ray crystallographic structure of Chrimson (PDB ID: 5ZIH [24]). The TM3 motif residues and the lysine residue in TM7 binding to the retinal chromophore are shown by blue diamonds and a green star, respectively.

In this study, we found a new channelrhodopsin-like gene through freshwater metatranscriptomic sampling in Lake Hula, Israel. We biophysically characterized this protein by heterologously expressing in mammalian cells and compared its characteristics with those of Chrimson to clarify the color tuning mechanisms in these proteins.

Materials and methods

Sampling, RNA extraction, and metatranscriptome assembly

The details of metatranscriptome sampling was reported previously [25]. Peat lake sampling was performed on February 23rd, 2021 in The Hula Nature Reserve, Israel (33°04'33.8"N 35°36'40.8"E). 20 L of water from the surface and 0.5 m depth was filtered through a 50 µm mesh net to remove large particles, filtered onto a GF/D filter (Whatman), and flash-frozen using liquid nitrogen on-site.

Total RNA was extracted from frozen filters, corresponding to ~5 L per sample (RNeasy PowerSoil Total RNA Kit; Qiagen). The RNA was tested with Bioanalyzer, and PolyA-selected libraries were constructed and sequenced at the Weizmann Institute of Science, on the NovaSeq platform (300 cycles, PE).

De-Novo assembly was done post trimming (Trimgalore; v. 0.6.6) [26], Cutadapt v. 3.4 [27] with MEGAHIT (v. 1.2.9) [28] and then clustered to reduce redundancy with cd-hit-est v. 4.8.1 [29]. An initial rhodopsin screening was done with HMMsearch (v. 3.3.2) [30] with the microbial rhodopsin profiles from https://github.com/BejaLab/RhodopsinProfiles.

DNA constructs for electrophysiology

The sequence of full-length HulaChrimson was cloned into pCMV3.0-enhanced fluorescent yellow protein (EYFP) vector (Supplementary Table S1). The QuikChange® site-directed mutagenesis method (Agilent Technologies, CA) was employed for point mutations. The sequences of primers used for site-directed mutagenesis are listed in Supplementary Table S2.

UV–visible spectroscopy

Cell culture and transfection for UV–visible spectroscopy were performed following the procedure outlined in previous studies [31]. COS-1 cells (cell line: JCRB9082; Japanese Collection of Research Bioresources Cell Bank, Japan) were transfected using the polyethyleneimine method [32]. The following day, the cells were supplemented with 2.5 µM ATR and harvested 48 hours after transfection. The cell membranes were solubilized with a buffer containing 66.5 mM phosphate (pH 7.0), 133 mM NaCl, and 3% *n*-dodecyl-β-D-maltoside. After centrifugation (21,600 ×*g*, 10 min, 20 °C), the supernatant was collected and used to measure the UV–visible absorption spectra using a spectrophotometer (V-730, JASCO, Japan). Rhodopsin was bleached via hydrolysis of the Schiff-base linkage of the retinal chromophore using hydroxylamine (50 mM, final concentration) under visible light from a 1-kW Xe lamp (MAX-303, Asahi Spectra, Japan) through a long-pass filter (Y52, AGC Techno Glass, Japan). Difference spectra were obtained by subtracting the post-illumination spectra from the pre-illumination spectra.

Cell culture and transfection for electrophysiology

ND7/23 cells, which are hybrid cell lines derived from neonatal rat dorsal root ganglia neurons fused with mouse neuroblastoma, were cultured in Dulbecco's modified Eagle's medium (D-MEM, FUJIFILM Wako Pure Chemical Co., Japan) supplemented with 5% fetal bovine serum (FBS) and maintained under a 5% CO_2 atmosphere at 37 °C. ND7/23 cells were plated onto collagen-coated 12-mm coverslips (IWAKI, cat. 4912–010, Japan) placed in a 4-well cell culture plate (SPL Life Sciences, cat. 30004, Korea). The expression plasmids were transfected into ND7/23 cells using Lipofectamine® 3000 transfection reagent (Thermo Fisher Scientific Inc., MA). Six to seven hours after the transfection, the medium was replaced with D-MEM containing 10% horse serum (New Zealand origin, Thermo Fisher Scientific Inc., MA), 50 ng/mL nerve growth factor-7S (Sigma-Aldrich, MO), 1 mM N6,2′-O-dibutyryladenosine-3′,5′-cyclic monophosphate sodium salt (Nacalai Tesque, Japan), 1 µM cytosine-1-β-D(+)-arabinofuranoside (FUJIFILM Wako Pure Chemical Co., Japan), and 2.5 µM ATR (Toronto Research Chemicals, ON, Canada). Electrophysiological recordings were performed 2–3 days after transfection. The transfected cells were identified by observing the EYFP fluorescence using an upright microscope (BX50WI, Olympus, Japan).

Electrophysiology

All experiments were performed at 20–22 °C. Currents were measured using an EPC-8 amplifier (HEKA Electronic, Germany) with a whole-cell patch clamp setup. The data were filtered at 1 kHz, sampled at 50 kHz (Digidata1440 A/D, Molecular Devices, CA), and saved to a computer (pClamp11.1, Molecular Devices, CA).

The standard internal pipette solutions for the whole-cell voltage clamp recordings from the ND7/23 cells contained 120 mM NaOH, 90 mM glutamate, 2.5 mM $MgCl_2$, 5 mM Na_2EGTA, 45 mM HEPES (pH 7.4 adjusted with HCl), 2.5 mM Mg-ATP. The standard extracellular solution contained 138 mM NaCl, 3 mM KCl, 2.5 mM $CaCl_2$, 1 mM $MgCl_2$, 10 mM HEPES (pH 7.4 adjusted with HCl), 4 mM NaOH, and 11 mM glucose.

In the ion selectivity measurements, the extracellular solution consisted of 146 mM NaCl or KCl, 6 mM N-methyl-D-glucamine (NMG), 2.5 mM $CaCl_2$, 10 mM HEPES (pH 7.4, adjusted with HCl), and 11 mM glucose. The NMG-extracellular solution consisted of 146 mM NMG, 146 mM HCl, 2.5 mM $CaCl_2$, 10 mM HEPES (pH 7.4, adjusted with

NMG), and 11 mM glucose. The NMG-pipette solution consisted of 130 mM NMG, 90 mM glutamate, 6 mM $(NMG)_2EGTA$, 50 mM HEPES (pH 7.4, adjusted with H_2SO_4), 2.5 mM $MgSO_4$, 2.5 mM MgATP, and 2.5 μM ATR. The liquid junction potentials (LJPs) were calculated by pClamp 11.1 software based on the compositions of extracellular and pipette solutions, and intrinsic reversal potentials (E_{rev}) were determined by correcting apparent reversal potentials (E_{rev}^{app}) using calculated LJPs as follows:

$$E_{rev} = E_{rev}^{app} - LJP$$

For measuring the pH dependence of the *I–V* curve, the components of the extracellular solutions were based on the standard extracellular solution described above, with 10 mM HEPES replaced by 2-morpholinoethanesulfonic acid (MES) at pH 6.0, or by N-cyclohexyl-2-aminoethanesulfonic acid (CHES) at pH 9.0. For whole-cell voltage clamp, illumination at wavelengths of 377 ± 25, 438 ± 12, 472 ± 15, 510 ± 5, 542 ± 13, 575 ± 12, or 643 ± 10 nm was provided using a SpectraX light engine (Lumencor Inc., OR), controlled by pClamp 11.1 software. The membrane potential was set to −40 mV, and multiple light exposures with varying intensities of 510-nm light were applied. The light intensity at which the current reached half of the maximum current indicated by rhodopsin was used as the light intensity for the action spectrum. The action spectrum was measured with light intensities in the range of 1.50–1.59 mW/mm², and the membrane potential was set to −40 mV.

Results

Electrophysiological characterization of HulaChrimson

A phylogenetic analysis suggests that the amino acid sequence of the new rhodopsin gene sampled in Lake Hula is highly similar to that of Chrimson (Accession number: AHH02126) [22] in the chlorophyte CCR clade (Figure 1A, 1B). The sequence identity and homology between these two proteins, except for their highly diversified N- and C-termini, are 53.8% and 74.6%, respectively (Figure 1C and Supplementary Figure S1), placing them in proximity in the phylogenetic tree (Figure 1A). Based on the high similarity of its primary sequence to Chrimson, we named this newly discovered rhodopsin from Lake Hula as "HulaChrimson". The Alphafold 3 [33] predicted structure of HulaChrimson exhibits seven transmembrane architecture (TM1–TM7) and β-strand in the first extracellular loop and the C-terminus, which is also highly similar to those of Chrimson (PDB ID: 5ZIH [24]) (Figure 1B).

To electrophysiologically characterize the ion-transporting properties of HulaChrimson, the protein C-terminally fused with EYFP and expressed in ND7/23 cells exhibited fluorescence from the outlines of the cell (Figure 2A). The lack of significant fluorescence of EYFP inside the cells indicates that HulaChrimson is almost exclusively localized in the plasma membranes, which is beneficial for optogenetics application.

Upon 510-nm light illumination, an inward photocurrent was observed at −80 mV holding potential (Figure 2B). The photocurrent intensity was decreased along with raising the holding potential, and it reverted to the positive current with a reversal potential (E_{rev}) = −1.1 ± 1.8 mV (mean ± S.E.). While E_{rev} was significantly shifted toward a negative value (E_{rev} = −21 ± 4 mV) upon replacing the standard bath solution with an NMG^+ bath solution (Figure 2B), it exhibits a more pronounced negative shift when the extracellular pH is increased from pH 6 to pH 9 (Figure 2C, and Supplementary Table S3). Additionally, inner and outer currents became larger at pH 6 and pH 9 compared to those at pH 7.4, respectively. These results indicate that HulaChrimson efficiently transports protons like Chrimson [23,34]. While the increased inward currents at pH 6 on the extracellular side can be attributed to the higher proton concentration compared to that on the intracellular side, the markedly increased outward photocurrents at pH 9—with a pipette solution identical to that used in the experiment at pH 7.4—suggest that the conductance of HulaChrimson is enhanced under extracellular alkaline conditions. The *I–V* curve recorded in the NMG^+ bath solution does not exhibit significant rectification at identical extracellular and intracellular pH, which is also similar to that observed in Chrimson [23,34] (Figure 2B). Since there is a significant difference in E_{rev} between bath solutions containing only Na^+, K^+ or NMG^+ (1.3 ± 1.8 mV, −9.1 ± 1.3 mV, and −21.5 ± 1.8 mV, respectively) (Supplementary Figure S2, and Supplementary Table S3), these results indicate that Na^+ and K^+ are also transported by HulaChrimson. Using the Goldman–Hodgkin–Katz (GHK) equation,

$$\Delta E_{\mathrm{rev}} = \frac{RT}{F} ln \left(\frac{P_X[X^+]_o + P_H[H^+]_o}{P_H[H^+]_o}\right),$$

and the difference in E_{rev} values (ΔE_{rev}), the relative cation selectivities of HulaChrimson for Na^+ and H^+ and for K^+ and H^+ were determined as $P_{Na+}/P_{H+} = 1.02^{+0.18}_{-0.16} \times 10^{-6}$ and $P_{K+}/P_{H+} = 0.43^{+0.10}_{-0.09} \times 10^{-6}$, respectively. This P_{Na+}/P_{H+} value is markedly higher than that of Chrimson ($P_{Na+}/P_{H+} = 0.07 \times 10^{-6}$ [34]), indicating the cation-transport pathway in HulaChrimson is not as highly proton-selective as Chrimson.

The photocurrent decay following light cessation was fitted with a double-exponential function characterized by two

time constants, $\tau_{off,fast}$ and $\tau_{off,slow}$ (Supplementary Table S4). The $\tau_{off,fast}$ and $\tau_{off,slow}$ values of the HulaChrimson WT, 28.3 ± 0.3 ms and 432 ± 5 ms at +60 mV holding potential, respectively, are similar to the channel-closing time of Chrimson [22-24,34]. Interestingly, the channel-closing decelerated at higher pH (Figure 2C), which is also similar to that observed for Chrimson, indicating the channel-closing mechanism coupled with proton concentrations is conserved between these two proteins [22-24,34].

Then, we investigated the light-intensity dependence of the photocurrents of HulaChrimson. While the rise in photocurrents was accelerated by increasing light intensity, a gradual decrease in photocurrents during the illumination period was observed at intensity > 0.2 mW/mm^2 (Supplementary Figure S3). This prolonged decrease in photocurrents without sharp peak currents, which are typically seen in many chlorophyte CCRs [21,22,35], under highly conductive conditions with strong light is likely due to changes in intracellular pH through the H^+ channel activity of HulaChrimson as observed for Chrimson [34].

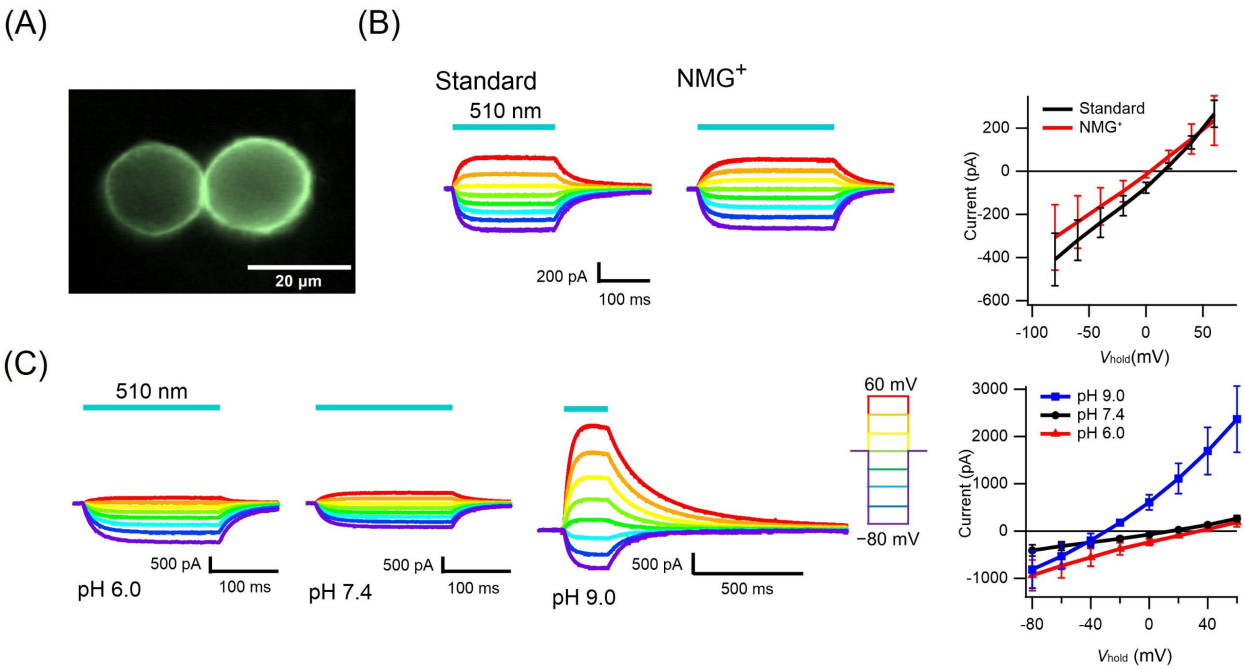

Figure 2 Electrophysiological characterization of HulaChrimson expressed in ND7/23 cells.
(A) Fluorescence image of HulaChrimson, which is labeled with EYFP (Scale bar = 20 µm), expressed in ND7/23 cells. (B) The *I-V* plots of HulaChrimson photocurrents with standard (black) and NMG^+ (red) bath solutions (mean ± S.E., n = 5). (C) The *I-V* plots of HulaChrimson photocurrents at different extracellular pH (mean ± S.E., n = 5).

Next, the action and absorption spectra of HulaChrimson were investigated. The photocurrents peaked at 510-nm excitation wavelength (Figure 3A). This action spectrum of HulaChrimson is significantly blue-shifted compared to that of Chrimson, which peaks at ~590 nm [22,34]. Moreover, we estimated the maximum absorption wavelength (λ_{max}) of HulaChrimson by calculating the difference absorption spectra upon bleaching of protein using hydroxylamine to hydrolyze the Schiff base linkage of the ATR chromophore. As a result, a positive peak representing the absorption of the original protein was observed at 501 nm (Figure 3B), which is 60–80 nm shorter than the λ_{max} of purified Chrimson (562–580 nm) [24]. Given the high similarity between HulaChrimson and Chrimson, these results suggest that the λ_{max} can be tuned over a wide range by differences in a limited number of residues in these proteins.

To elucidate the reason for this highly blue-shifted absorption of HulaChrimson despite its sequence highly similar to Chrimson, we focused on seven amino acid residues, which differ between HulaChrimson and Chrimson and exhibit significantly different chemical properties: T188 (S169 in Chrimson) and H195 (K176), which are the second and third TM3-motif residues known for playing essential roles in determining the functionality of many microbial rhodopsins [3,36,37] , as well as C183 (F164), V217 (C198), T288 (P269), S317 (A298), and Q319 (E300) (Figure 1B, 1C, and Supplementary Figure S1). To identify the residues critical for the difference in the λ_{max} between HulaChrimson and Chrimson, we introduced mutations in HulaChrimson, replacing these residues with their corresponding amino acids in Chrimson. If the residues responsible for HulaChrimson's blue-shifted absorption are mutated, it would result in the red-

shift of the action and absorption spectra.

Among seven mutants, only HulaChrimson S317A exhibited significantly red-shifted action and absorption spectra (Figure 3). While photocurrents were enhanced at 542- and 575-nm excitation and reduced at 472-nm excitation (Figure 3A), its λ_{max} was estimated to be 517 nm, which is 16 nm longer than that of the WT (Figure 3B). By contrast, HulaChrimson T288P exhibited a blue-shift in the spectra (Figure 3). It is known that substituting a proline at this position—corresponding to P269 and P186 in Chrimson and *Hs*BR, respectively with a threonine induces 6–20 nm red-shifts in ion-transporting rhodopsins [20,38]. While our results indicate that T288 exhibits a similar 8-nm red-shifting effect in HulaChrimson, the difference of amino acid at this position is not the cause of HulaChrimson's blue-shifted absorption compared to that of Chrimson. Notably, the channel-closing process of T288P is significantly slower than that of the WT (Supplementary Figure S4A). Both of $\tau_{off,fast}$ and $\tau_{off,slow}$ of HulaChrimson T288P ($\tau_{off,fast}$ = 312 ± 3 ms and $\tau_{off,slow}$ = 2.4 ±

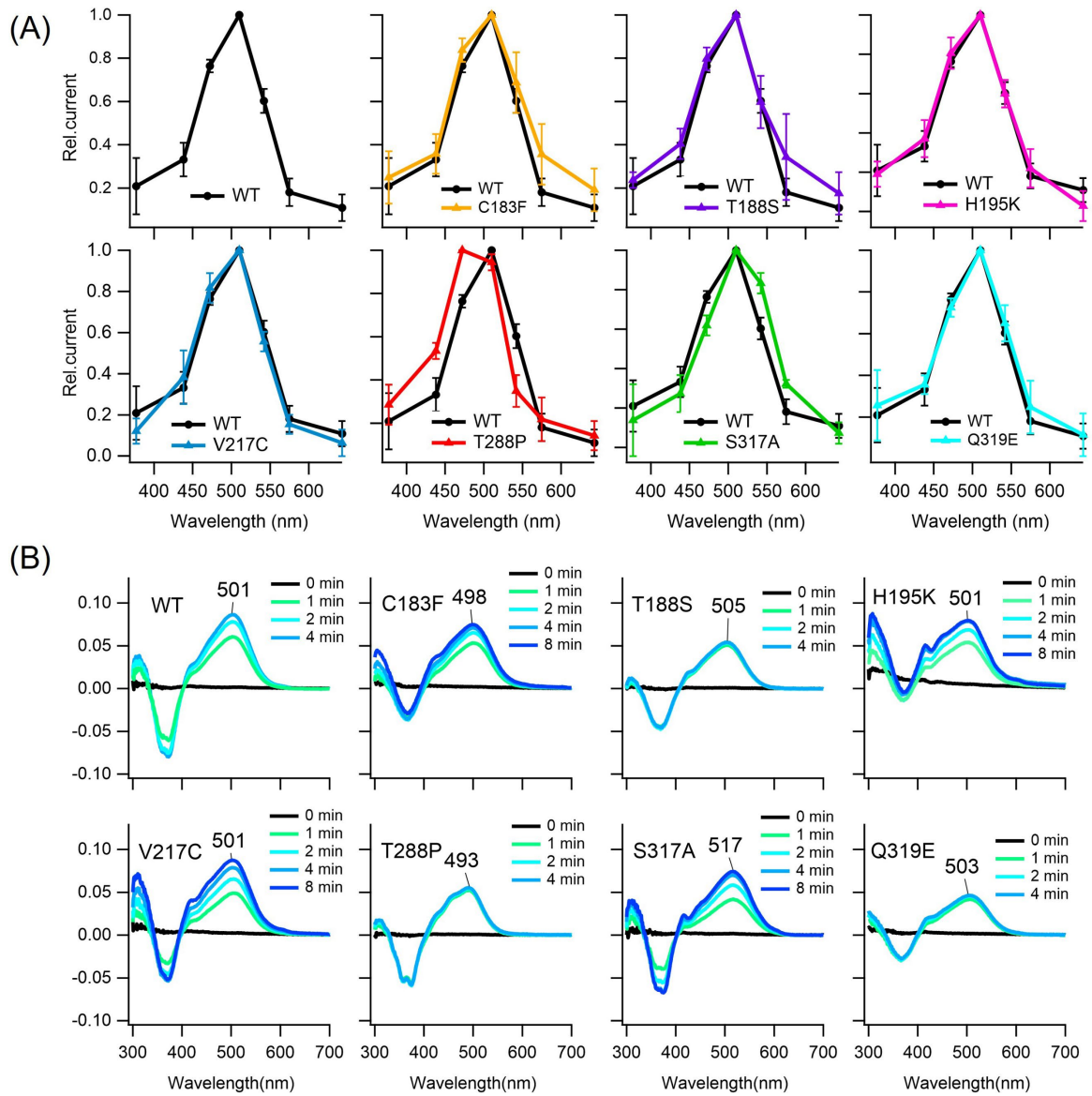

Figure 3 Action and UV–visible absorption spectra of HulaChrimson mutants.
(A) Action spectra of HulaChrimson WT and mutants (mean ± S.E., n = 5). To record photocurrents, cells were illuminated with light at 377 ± 25, 438 ± 12, 472 ± 15, 510 ± 5, 542 ± 13, 575 ± 12, 643 ± 10 nm, and photocurrents are normalized at 510 nm. (B) Difference absorption spectra calculated by subtracting the spectra after the hydroxylamine bleaching of HulaChrimson WT and mutants from the spectra before bleaching. Illumination times (0, 1, 2, 4, and 8 min) were indicated by different colors.

0.2 s at +60 mV holding potential) are significantly longer than those of the WT ($\tau_{off,fast}$ = 28.3 ± 0.3 ms and $\tau_{off,slow}$ = 432 ± 5 ms). The λ_{max} of other mutants are identical to that of the WT, indicating their mutated residue cannot be solely the cause of the λ_{max} difference between HulaChrimson and Chrimson. Notably, HulaChrimson T188S, T288P, and Q319E were more quickly bleached compared to the WT, suggesting the accessibility of hydroxylamine to the retinal Schiff base (RSB) is increased by structural alteration of the protein caused by these mutations. HulaChrimson C183F exhibited $\tau_{off,fast}$ and $\tau_{off,slow}$ significantly slower than that of the WT, which indicates that this residue also contributes to the fast channel gating in HulaChrimson (Supplementary Figure S4 and Supplementary Table S4).

Beside having absorption spectra identical to that of the WT, V217C exhibited the prolonged fast channel-closing component $\tau_{off,fast}$ ($\tau_{off,fast}$ = 187 ± 2 ms at +60 mV holding potential) (Supplementary Figure S4). Interestingly, V217 in TM4 is located at the position corresponding to D156 in *Cr*ChR2, which interacts with C128 in TM3 to form the so-called DC gate, a critical structural element that regulates channel kinetics [14,39]. In the crystal structure of *Cr*ChR2, D156 and C128 interact through a hydrogen bonding network mediated by a water molecule [40], and disruption of this interaction leads to a strong deceleration of channel closing [39]. Because a hydrogen bond cannot form between V217 and C189 in HulaChrimson, the $\tau_{off,fast}$ of HulaChrimson remains short through a mechanism distinct from that of *Cr*ChR2, as has also been suggested also for Chrimson [24].

Discussion

In this study, we characterized HulaChrimson, which was found in Lake Hula and shares high sequence homology with Chrimson. Electrophysiological patch-clamp measurements clarified that while HulaChrimson significantly transport H^+, its Na^+ selectivity ($P_{Na+}/P_{H+} = 1.02^{+0.18}_{-0.16} \times 10^{-6}$) is markedly higher than that of Chrimson (0.07×10^{-6} [34]), similar to that of other chlorophyte CCRs such as *Cr*ChR2 ($0.46–1.0 \times 10^{-6}$ [35]), *Cr*ChR1 ($\sim 1.0 \times 10^{-6}$ [41]), and *Ps*ChR (2.3×10^{-6} [34]), but lower than that of cryptophyte CCRs like *Gt*CCR4 (50×10^{-6} [42]) and HulaCCR1 (15×10^{-6} [25]). The τ_{off} of both of HulaChrimson and Chrimson increases by raising extracellular pH [34] (Figure 2C). Additionally, the absence of sharp peak currents is another feature shared with Chrimson, suggesting that HulaChrimson and Chrimson share common mechanisms underlying their ion-channeling function despite the large difference in their absorption spectra. Transient absorption measurements of Chrimson observed the formation of a highly blue-shifted M-like P2_alk state, in which the retinal chromophore is deprotonated, at alkaline pH [23]. Since the decay time constants of P2_alk in Chrimson are close to those of channel closing, the conversion of P2_alk to the subsequent red-shifted P3_alk corresponds to the channel closing, and similar mechanisms may underlay the long τ_{off} of HulaChrimson at pH 9.0. Mutation of K176 on the cytoplasmic side of TM4 in Chrimson to a histidine residue eliminates the extracellular pH dependence of τ_{off} [34]. In HulaChrimson, H195 occupies the same position (Supplementary Figure S1), suggesting that the structural environment around this residue differs between HulaChrimson and Chrimson, and that another residue is responsible for the pH-dependent channel closing in the former. Notably, significant steady-state photocurrent attenuation—so-called desensitization—was observed under high-intensity light (>0.68 mW/mm^2, Supplementary Figure S3), whereas a similar phenomenon does not occur in Chrimson [34]. In many ChRs—as most extensively studied in *Cr*ChR2 [43-45]—steady-state photocurrent attenuation is associated with the accumulation of a long-lived intermediate state that contributes less efficiently to ion conductance. The distinct desensitization behaviors of HulaChrimson and Chrimson under high-intensity illumination may be attributable to difference in their photointermediate states, which lead to the formation of a less conductive state upon absorption of excitation light in HulaChrimson. Therefore, mechanisms underlying the pronounced desensitization of HulaChrimson will be further investigated through spectroscopic analysis of the photointermediate state in its photocycle using purified protein in future studies. The photointermediate states of HulaChrimson are expected to significantly differ from those of Chrimson at neutral pH, where E165 (corresponding to E184 in HulaChrimson) is protonated [23]. E139 and E143—also referred to E4' and E5' representing the fourth and fifth residues in five highly conserved glutamic acid residues among Chlorophyte CCRs—in Chrimson is critical for its high H^+ selectivity [34]. Interestingly, the latter is replaced with a histidine residue (H161) in HulaChrimson, suggesting that the structure of the extracellular selective filter is distinct from that in Chrimson. Notably, the outward photocurrents were markedly enhanced by increasing the extracellular pH from 7.4 to 9.0—a phenomenon not observed for Chrimson [34]. This result suggests that the conductance of HulaChrimson is enhanced under extracellular alkaline conditions, probably due to the deprotonation of an unidentified extracellular residue. The origin of this extracellular pH-dependent photocurrent will be investigated through comprehensive mutational analysis and three-dimensional structural studies.

In Chrimson and channelrhodopsin1 from *Chlamydomonas augustae* (*Ca*ChR1), E165 and E169, which correspond to E184 in HulaChrimson, respectively, are substantially protonated at neutral pH [23,46]. This protonation of the counterion in TM3 is considered as the main reason for the red-shifted absorption of these CCRs [23,46]. Additionally, the substitution of a lysine residue conserved in many CCRs—such as K93 in *Cr*ChR2—with non-charged residues has been suggested to be critical for their red-shifted absorption and the high pK_a of the primary counterion in TM3 (Figure 1C and Supplementary Figure S1) [23,46]. Interestingly, HulaChrimson also has a phenylalanine (F154), like Chrimson and

*Ca*ChR1, suggesting that the pK_a of its counterion in TM3, E184, remains low through a mechanism distinct from that in many chlorophyte CCRs—likely due to differences in the electrostatic and hydrogen-bonding architecture in the RSB region. Moreover, E139 (E4') and Y159, located in the vicinity of F135, also contribute to the high pK_a of E165 in Chrimson [34]. Since these residues are conserved in HulaChrimson (E158 and Y178), the origin of the different pK_a of the counterion in TM3 between HulaChrimson and Chrimson must be attributed to other parts within the proteins.

The red shift observed for HulaChrimson S317A mutation without affecting photocurrent intensity (Supplementary Figure S4) suggests that this serine was evolved to red shift the absorption in HulaChrimson in nature. By contrast, the T288P mutation affects both the λ_{max} and τ_{off} (Figure 3 and Supplementary Figure S4). Notably, HulaChrimson has a TxTxxT motif in TM6, where the three threonine residues correspond to T283, T285, and T288 (Supplementary Figure S5). Such Thr/Ser motifs in hydrophobic environments are known to influence the local structure and dynamics of α helices through hydrogen bonding interactions between the side chains of Thr/Ser and the main chain of neighboring α-helical turns [47]. The increase in τ_{off} upon the T288P mutation suggests that T288 regulates the local structure and the dynamics of TM6 to facilitate rapid channel closing. Because this TxTxxT motif is absent in *Cr*ChR2 and Chrimson, it is likely to have evolved in HulaChrimson.

In Chrimson, a mutation of E300 to a glutamine residue results in a large blue shift to λ_{max} = 519 nm, whereas mutations to asparagine or alanine significantly decelerate channel closing [24,34]. By contrast, the reverse mutation Q319E in HulaChrimson does not significantly affect either the λ_{max} or photocurrent properties (Figure 3 and Supplementary Figure S4), suggesting structural differences around this residue between Chrimson and HulaChrimson Q319E. In *Cr*ChR2 and C1C2, a chimeric CCR derived from *Cr*ChR1 and *Cr*ChR2, asparagine residues N258 and N297, respectively, occupy the corresponding position, where they form a hydrogen bond with serine residues S63 and S102 in TM1 [40,48]. By contrast, in Chrimson, S63/S102 in *Cr*ChR2/C1C2 are replaced with A105, preventing hydrogen bond formation with E300. This leads to the formation of an alternative hydrogen bond between E300 and the main-chain carbonyl group of A101, which is located one α-helical turn extracellular to A105 [24]. In HulaChrimson, C124 is located at the position of A105 in Chrimson. It may interact with E319 in the Q319E mutant, leading to a structure distinct from that of Chrimson by preventing the interaction between E319 and the main chain of TM1. Since elucidating such a broad network of interactions is difficult without the three-dimensional structure of the protein, a single-particle analysis using cryo-electron microscopy and/or X-ray crystallography of HulaChrimson will be performed in the near future.

Conclusion

Through freshwater metatranscriptome sampling in Lake Hula, Israel, we identified a new Chrimson-like protein, HulaChrimson. Despite its amino acid sequence being highly similar to that of Chrimson, the action and absorption spectra of HulaChrimson are 60–80 nm blue-shifted compared to those of Chrimson. While the mutational study, in which characteristic amino acid residues were substituted to the amino acid identical to those in Chrimson, revealed that 16 nm blue-shift is caused by the difference between serine and alanine at 317th position, the primary cause of the overall blue shift remains unknown. To achieve a more precise understanding, three-dimensional structural analysis of HulaChrimson will be conducted in the near future.

Conflict of interest

The authors declare that they have no conflict of interest.

Author contributions

S.F., A.R., and O.B. performed freshwater metatranscriptomic sampling and analysis. H.T. and T.N. cultured COS-1 and ND7/23 cells for HulaChrimson expression. H.T. and T.N. produced the DNA constructs for HulaChrimson expression and carried out hydroxylamine-bleaching experiments. H.T. and S.T. carried out patch-clamp measurements. All authors co-wrote the manuscript. K.I. directed the entire project.

Data availability

The evidence data generated and/or analyzed during the current study areavailable from the corresponding author on reasonable request.

Acknowledgements

The authors appreciate Dr. Andrey Rozenberg at Technion — Israel Institute of Technology for his insightful comments.

This work was supported by JSPS KAKENHI Grants-in-Aid (Grant Number: JP24K23073 to Y.K., JP23K21092, JP23K18090, JP23H04404, and JP24H02268, to K.I.), JST CERST (Grant Number: JPMJCR22N2 to K.I.), and MEXT Promotion of Development of a Joint Usage/ Research System Project: Coalition of Universities for Research Excellence Program (CURE) (Grant Number: JPMXP1323015482 to K.I.), the European Commission, under Horizon Europe's research and innovation programme (Bluetools project, Grant Agreement No 101081957 to O.B.), the Israel Science Foundation (Research Center grant 3131/20 to O.B.), and the Nancy and Stephen Grand Technion Energy Program (GTEP). O.B. holds the Louis and Lyra Richmond Chair in Life Sciences.

References

[1] Ernst, O. P., Lodowski, D. T., Elstner, M., Hegemann, P., Brown, L. S., Kandori, H. Microbial and animal rhodopsins: Structures, functions, and molecular mechanisms. Chem. Rev. 114, 126–163 (2014). https://doi.org/10.1021/cr4003769

[2] Rozenberg, A., Inoue, K., Kandori, H., Béjà, O. Microbial rhodopsins: The last two decades. Annu. Rev. Microbiol. 75, 427–447 (2021). https://doi.org/10.1146/annurev-micro-031721-020452

[3] Nagata, T., Inoue, K. Rhodopsins at a glance. J. Cell Sci. 134, jcs258989 (2021). https://doi.org/10.1242/jcs.258989

[4] Nagel, G., Ollig, D., Fuhrmann, M., Kateriya, S., Musti, A. M., Bamberg, E., et al. Channelrhodopsin-1: A light-gated proton channel in green algae. Science 296, 2395–2398 (2002). https://doi.org/10.1126/science.1072068

[5] Govorunova, E. G., Sineshchekov, O. A., Li, H., Spudich, J. L. Microbial rhodopsins: Diversity, mechanisms, and optogenetic applications. Annu. Rev. Biochem. 86, 845–872 (2017). https://doi.org/10.1146/annurev-biochem-101910-144233

[6] Boyden, E. S., Zhang, F., Bamberg, E., Nagel, G., Deisseroth, K. Millisecond-timescale, genetically targeted optical control of neural activity. Nat. Neurosci. 8, 1263–1268 (2005). https://doi.org/10.1038/nn1525

[7] Ishizuka, T., Kakuda, M., Araki, R., Yawo, H. Kinetic evaluation of photosensitivity in genetically engineered neurons expressing green algae light-gated channels. Neurosci. Res. 54, 85–94 (2006). https://doi.org/10.1016/j.neures.2005.10.009

[8] Deisseroth, K., Hegemann, P. The form and function of channelrhodopsin. Science 357, eaan5544 (2017). https://doi.org/10.1126/science.aan5544

[9] Deisseroth, K. Optogenetics: 10 years of microbial opsins in neuroscience. Nat. Neurosci. 18, 1213–1225 (2015). https://doi.org/10.1038/nn.4091

[10] Kianianmomeni, A., Stehfest, K., Nematollahi, G., Hegemann, P., Hallmann, A. Channelrhodopsins of *Volvox carteri* are photochromic proteins that are specifically expressed in somatic cells under control of light, temperature, and the sex inducer. Plant Physiol. 151, 347–366 (2009). https://doi.org/10.1104/pp.109.143297

[11] Wang, H., Sugiyama, Y., Hikima, T., Sugano, E., Tomita, H., Takahashi, T., et al. Molecular determinants differentiating photocurrent properties of two channelrhodopsins from *Chlamydomonas*. J. Biol. Chem. 284, 5685–5696 (2009). https://doi.org/10.1074/jbc.M807632200

[12] Berndt, A., Lee, S. Y., Ramakrishnan, C., Deisseroth, K. Structure-guided transformation of channelrhodopsin into a light-activated chloride channel. Science 344, 420–424 (2014). https://doi.org/10.1126/science.1252367

[13] Wietek, J., Wiegert, J. S., Adeishvili, N., Schneider, F., Watanabe, H., Tsunoda, S. P., et al. Conversion of channelrhodopsin into a light-gated chloride channel. Science 344, 409–412 (2014). https://doi.org/10.1126/science.1249375

[14] Schneider, F., Grimm, C., Hegemann, P. Biophysics of channelrhodopsin. Annu. Rev. Biophys. 44, 167–186 (2015). https://doi.org/10.1146/annurev-biophys-060414-034014

[15] Govorunova, E. G., Sineshchekov, O. A., Janz, R., Liu, X., Spudich, J. L. Natural light-gated anion channels: A family of microbial rhodopsins for advanced optogenetics. Science 349, 647–650 (2015). https://doi.org/10.1126/science.aaa7484

[16] Govorunova, E. G., Sineshchekov, O. A., Spudich, J. L. Structurally distinct cation channelrhodopsins from cryptophyte algae. Biophys. J. 110, 2302–2304 (2016). https://doi.org/10.1016/j.bpj.2016.05.001

[17] Yamauchi, Y., Konno, M., Ito, S., Tsunoda, S. P., Inoue, K., Kandori, H. Molecular properties of a dtd channelrhodopsin from *Guillardia theta*. Biophys. Physicobiol. 14, 57–66 (2017). https://doi.org/10.2142/biophysico.14.0_57

[18] Marshel, J. H., Kim, Y. S., Machado, T. A., Quirin, S., Benson, B., Kadmon, J., et al. Cortical layer-specific critical dynamics triggering perception. Science 365, eaaw5202 (2019). https://doi.org/10.1126/science.aaw5202

[19] Govorunova, E. G., Sineshchekov, O. A., Li, H., Wang, Y., Brown, L. S., Spudich, J. L. RubyACRs, nonalgal anion channelrhodopsins with highly red-shifted absorption. Proc. Natl. Acad. Sci. U.S.A. 117, 22833–22840 (2020). https://doi.org/10.1073/pnas.2005981117

[20] Kojima, K., Miyoshi, N., Shibukawa, A., Chowdhury, S., Tsujimura, M., Noji, T., et al. Green-sensitive, long-lived, step-functional anion channelrhodopsin-2 variant as a high-potential neural silencing tool. J. Phys. Chem. Lett. 11, 6214–6218 (2020). https://doi.org/10.1021/acs.jpclett.0c01406
[21] Tashiro, R., Sushmita, K., Hososhima, S., Sharma, S., Kateriya, S., Kandori, H., et al. Specific residues in the cytoplasmic domain modulate photocurrent kinetics of channelrhodopsin from *Klebsormidium nitens*. Commun. Biol. 4, 235 (2021). https://doi.org/10.1038/s42003-021-01755-5
[22] Klapoetke, N. C., Murata, Y., Kim, S. S., Pulver, S. R., Birdsey-Benson, A., Cho, Y. K., et al. Independent optical excitation of distinct neural populations. Nat. Methods 11, 338–346 (2014). https://doi.org/10.1038/nmeth.2836
[23] Urmann, D., Lorenz, C., Linker, S. M., Braun, M., Wachtveitl, J., Bamann, C. Photochemical properties of the red-shifted channelrhodopsin Chrimson. Photochem. Photobiol. 93, 782–795 (2017). https://doi.org/10.1111/php.12741
[24] Oda, K., Vierock, J., Oishi, S., Rodriguez-Rozada, S., Taniguchi, R., Yamashita, K., et al. Crystal structure of the red light-activated channelrhodopsin Chrimson. Nat. Commun. 9, 3949 (2018). https://doi.org/10.1038/s41467-018-06421-9
[25] Takaramoto, S., Fainsod, S., Nagata, T., Rozenberg, A., Béjà, O., Inoue, K. Hulaccr1, a pump-like cation channelrhodopsin discovered in a lake microbiome. J. Mol. Biol. 436, 168844 (2024). https://doi.org/10.1016/j.jmb.2024.168844
[26] Krueger, F., James, F., Ewels, P., Afyounian, E., Weinstein, M., Schuster-Boeckler, B., et al. Felixkrueger/trimgalore: V0.6.10 - add default decompression path. Zenodo (2023). https://doi.org/10.5281/zenodo.7598955
[27] Martin, M. Cutadapt removes adapter sequences from high-throughput sequencing reads. EMBnet J. 17, 10–12 (2011). https://doi.org/10.14806/ej.17.1.200
[28] Li, D., Liu, C. M., Luo, R., Sadakane, K., Lam, T. W. MEGAHIT: An ultra-fast single-node solution for large and complex metagenomics assembly via succinct *de Bruijn* graph. Bioinformatics 31, 1674–1676 (2015). https://doi.org/10.1093/bioinformatics/btv033
[29] Li, W., Godzik, A. Cd-hit: A fast program for clustering and comparing large sets of protein or nucleotide sequences. Bioinformatics 22, 1658–1659 (2006). https://doi.org/10.1093/bioinformatics/btl158
[30] Johnson, L. S., Eddy, S. R., Portugaly, E. Hidden markov model speed heuristic and iterative hmm search procedure. BMC Bioinformatics 11, 431 (2010). https://doi.org/10.1186/1471-2105-11-431
[31] Morimoto, N., Nagata, T., Inoue, K. Reversible photoreaction of a retinal photoisomerase, retinal G-protein-coupled receptor RGR. Biochemistry 62, 1429–1432 (2023). https://doi.org/10.1021/acs.biochem.3c00084
[32] Fay, J. F., Farrens, D. L. Purification of functional CB_1 and analysis by site-directed fluorescence labeling methods. Methods Enzymol. 593, 343–370 (2017). https://doi.org/10.1016/bs.mie.2017.06.026
[33] Abramson, J., Adler, J., Dunger, J., Evans, R., Green, T., Pritzel, A., et al. Accurate structure prediction of biomolecular interactions with AlphaFold 3. Nature 630, 493–500 (2024). https://doi.org/10.1038/s41586-024-07487-w
[34] Vierock, J., Grimm, C., Nitzan, N., Hegemann, P. Molecular determinants of proton selectivity and gating in the red-light activated channelrhodopsin Chrimson. Sci. Rep. 7, 9928 (2017). https://doi.org/10.1038/s41598-017-09600-8
[35] Nagel, G., Szellas, T., Huhn, W., Kateriya, S., Adeishvili, N., Berthold, P., et al. Channelrhodopsin-2, a directly light-gated cation-selective membrane channel. Proc. Natl. Acad. Sci. U.S.A. 100, 13940–13945 (2003). https://doi.org/10.1073/pnas.1936192100
1936192100 [pii]
[36] Inoue, K., Kato, Y., Kandori, H. Light-driven ion-translocating rhodopsins in marine bacteria. Trends Microbiol. 23, 91–98 (2014). https://doi.org/10.1016/j.tim.2014.10.009
[37] Needham, D. M., Yoshizawa, S., Hosaka, T., Poirier, C., Choi, C. J., Hehenberger, E., et al. A distinct lineage of giant viruses brings a rhodopsin photosystem to unicellular marine predators. Proc. Natl. Acad. Sci. U.S.A. 116, 20574–20583 (2019). https://doi.org/10.1073/pnas.1907517116
[38] Inoue, K., Del Carmen Marin, M., Tomida, S., Nakamura, R., Nakajima, Y., Olivucci, M., et al. Red-shifting mutation of light-driven sodium-pump rhodopsin. Nat. Commun. 10, 1993 (2019). https://doi.org/10.1038/s41467-019-10000-x
[39] Yizhar, O., Fenno, L. E., Prigge, M., Schneider, F., Davidson, T. J., O'Shea, D. J., et al. Neocortical excitation/inhibition balance in information processing and social dysfunction. Nature 477, 171–178 (2011). https://doi.org/10.1038/nature10360
[40] Volkov, O., Kovalev, K., Polovinkin, V., Borshchevskiy, V., Bamann, C., Astashkin, R., et al. Structural insights into ion conduction by channelrhodopsin 2. Science 358, eaan8862 (2017). https://doi.org/10.1126/science.aan8862

[41] Berthold, P., Tsunoda, S. P., Ernst, O. P., Mages, W., Gradmann, D., Hegemann, P. Channelrhodopsin-1 initiates phototaxis and photophobic responses in *Chlamydomonas* by immediate light-induced depolarization. Plant Cell 20, 1665–1677 (2008). https://doi.org/10.1105/tpc.108.057919

[42] Shigemura, S., Hososhima, S., Kandori, H., Tsunoda, S. P. Ion channel properties of a cation channelrhodopsin, *Gt*_CCR4. Appl. Sci. 9, 3440 (2019). https://doi.org/10.3390/app9173440

[43] Nikolic, K., Grossman, N., Grubb, M. S., Burrone, J., Toumazou, C., Degenaar, P. Photocycles of channelrhodopsin-2. Photochem. Photobiol. 85, 400–411 (2009). https://doi.org/10.1111/j.1751-1097.2008.00460.x

[44] Saita, M., Pranga-Sellnau, F., Resler, T., Schlesinger, R., Heberle, J., Lorenz-Fonfria, V. A. Photoexcitation of the P_4^{480} state induces a secondary photocycle that potentially desensitizes channelrhodopsin-2. J. Am. Chem. Soc. 140, 9899–9903 (2018). https://doi.org/10.1021/jacs.8b03931

[45] Kuhne, J., Vierock, J., Tennigkeit, S. A., Dreier, M. A., Wietek, J., Petersen, D., et al. Unifying photocycle model for light adaptation and temporal evolution of cation conductance in channelrhodopsin-2. Proc. Natl. Acad. Sci. U.S.A. 116, 9380–9389 (2019). https://doi.org/10.1073/pnas.1818707116

[46] Li, H., Govorunova, E. G., Sineshchekov, O. A., Spudich, J. L. Role of a helix B lysine residue in the photoactive site in channelrhodopsins. Biophys. J. 106, 1607–1617 (2014). https://doi.org/10.1016/j.bpj.2014.03.002

[47] Del Val, C., White, S. H., Bondar, A. N. Ser/Thr motifs in transmembrane proteins: Conservation patterns and effects on local protein structure and dynamics. J. Membr. Biol. 245, 717–730 (2012). https://doi.org/10.1007/s00232-012-9452-4

[48] Kato, H. E., Zhang, F., Yizhar, O., Ramakrishnan, C., Nishizawa, T., Hirata, K., et al. Crystal structure of the channelrhodopsin light-gated cation channel. Nature 482, 369–374 (2012). https://doi.org/10.1038/nature10870